ADVANCED OPTICAL MATERIALS
www.advopticalmat.de

Electric and Magnetic Response in Dielectric Dark States for Low Loss Subwavelength Optical Meta Atoms

Aditya Jain, Parikshit Moitra, Thomas Koschny, Jason Valentine, and Costas M. Soukoulis*

Artificially created surfaces or metasurfaces, composed of appropriately shaped subwavelength structures, namely, meta-atoms, control light at subwavelength scales. Historically, metasurfaces have used radiating metallic resonators as subwavelength inclusions. However, while resonant optical metasurfaces made from metal have been sufficiently subwavelength in the propagation direction, they are too lossy for many applications. Metasurfaces made out of radiating dielectric resonators have been proposed to solve the loss problem, but are marginally subwavelength at optical frequencies. Here, subwavelength resonators made out of nonradiating dielectrics are designed. The resonators are decorated with appropriately placed scatterers, resulting in a meta-atom with an engineered electromagnetic response. As an example, a metasurface that yields an electric response is fabricated, experimentally characterized, and a method to obtain a magnetic response at optical frequencies is theoretically demonstrated. This design methodology paves the way for metasurfaces that are simultaneously subwavelength and low loss.

1. Introduction

Unlike photonic crystals, metamaterials derive their properties by modifying the electric and magnetic fields of light, and are free from diffraction.[1–8] The flexibility associated with the geometric control of metamaterials has resulted in fascinating applications such as perfect absorbers,[9] phase mismatch free nonlinear generation,[10] magnetic mirrors,[11,12] subwavelength cavities,[13] zero-index media,[14] and slow light devices.[15] To achieve these effects, the essential building blocks of a metamaterial, namely the meta-atoms, must be made sufficiently thin in the direction of propagation of the electromagnetic field. More recently, 2D versions of metamaterials or metasurfaces[16,17] have been proposed as an alternative to bulk 3D metamaterials due to their ease in fabrication, comparatively lower losses and small footprint for on-chip devices. The most popular construction materials for metasurfaces have been radiating metallic antennas,[5] although they have scaling issues at optical frequencies.[18] To circumvent this problem, radiating Mie resonances have been proposed in low loss high permittivity particles ($\varepsilon \approx 25$–1000) at GHz and lower THz frequencies.[19–24] However, straightforward scaling of this approach to optical frequencies renders isotropic meta-atoms, such as cubes and spheres, marginally subwavelength due to the absence of high index dielectrics.[25,26] Therefore, it is highly desirable to construct low loss meta-atoms made entirely out of dielectrics with modest permittivity ($\varepsilon \approx 2$–14), whilst still being sufficiently subwavelength in the propagation direction. Recently, researchers have experimented with silicon disks,[27,28] which can be more deeply subwavelength in the direction of propagation at telecommunication frequencies. However, these structures are still not sufficiently thin to compete with their metallic counterparts, especially when utilizing the magnetic response. As a reference, we have simulated the electric and magnetic response in a disk with radiating Mie resonance (see Figures S1 and S2, Supporting Information). An alternative approach is to access dark modes of the resonators,[29] which allow deeper subwavelength thicknesses while still preserving a sharp resonance, an approach that we will address in detail in this paper.

2. Polarization Dependent Electric Response

Two main loss channels in metamaterial resonators are present. The first loss channel is the dissipation, which can be reduced by choosing low loss dielectrics. The other loss channel, the radiative loss, can be reduced by suppressing the dipole moment of the resonator. Such nonradiative resonators

A. Jain, Dr. T. Koschny, Prof. C. M. Soukoulis
Ames Laboratory–U.S. DOE
Iowa State University
Ames, IA 50011, USA
E-mail: ajain17@iastate.edu
A. Jain
Department of Electrical and Computer Engineering
Iowa State University
Ames, IA 50011, USA
P. Moitra
Interdisciplinary Materials Science Program
Vanderbilt University
Nashville, TN 37212, USA
Dr. T. Koschny, Prof. C. M. Soukoulis
Department of Physics and Astronomy
Iowa State University
Ames, IA 50011, USA
Prof. J. Valentine
Department of Mechanical Engineering
Vanderbilt University
Nashville, TN 37212, USA
Prof. C. M. Soukoulis
Institute of Electronic Structure and Lasers (IESL)
FORTH, 71110 Heraklion, Crete, Greece

DOI: 10.1002/adom.201500222

are more commonly known as "dark" resonators.[30] This is generally achieved by choosing an appropriate geometry such that the overlap integral of the excited mode and the incident wave is negligible. Another advantage of using dark resonators is that they can be made sufficiently subwavelength in the propagation direction since they do not possess any dipole moment of their own. However, there is a dichotomy in the fact that complete suppression of radiative losses also leads to no metamaterial response. In this article, we propose a method to solve this problem using nonresonant scatterers. The combination of a nonradiative resonator and an appropriate scatterer results in a hybrid meta-atom. We demonstrate a general recipe to achieve polarization dependent and independent electric response in a single layer metamaterial using such hybrid meta-atoms. Experimental results prove that such resonances can be excited within reasonably subwavelength structures. We then recycle these resonators with another set of scatterers to theoretically demonstrate a meta-atom with a magnetic response as well. All the subsequent discussions concern optical metasurfaces at telecommunication frequencies. We characterize the 2D array of nanostructures as thin sheets with dimensionless electric or magnetic surface susceptibility $\left(\chi_{se}^{(d)}, \chi_{sm}^{(d)}\right)$ (see the Supporting Information).

We start our discussion by demonstrating a meta-atom exhibiting an electric response. The first step in the design is to realize a resonator with negligible dipole moment commensurate with the incident wave. The structure is comprised of a silicon disk ($\varepsilon \approx 13.69$, t1 = 115 nm; **Figure 1**a,b) with an asymmetrically etched rectangular slot placed on a quartz substrate ($\varepsilon \approx 2.19$). The unit cell is periodically repeated in the X and Y directions to form a metasurface. The incident plane wave has an electric field polarized along the X direction with a propagation vector along the Z direction (Figure 1b). The dark mode in consideration is the lowest order Mie mode (magnetic dipole mode) in a homogeneous cylindrical disk. The mode frequency is fixed primarily by the radius R of the disk (inset Figure 1b).

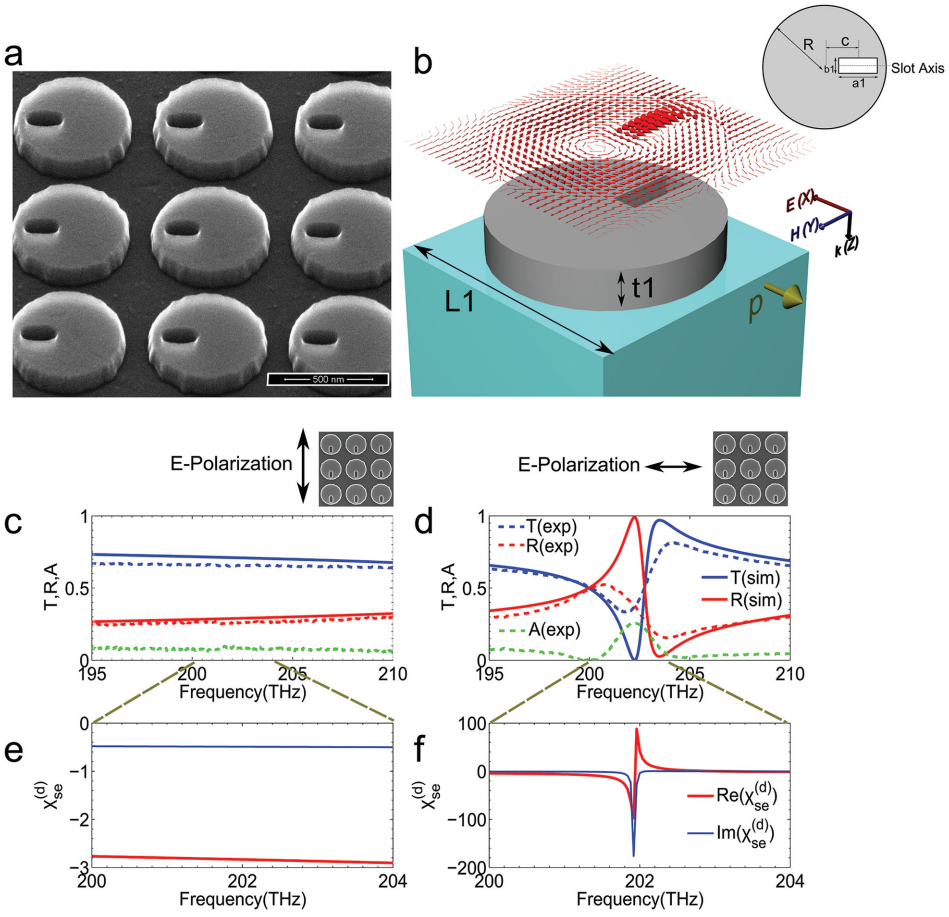

Figure 1. Polarization sensitive electric response of a dielectric disk with a rectangular slot. a) SEM image of a single layer dielectric disk based metamaterial with an asymmetric through slot. b) Simulated unit cell of the proposed design with a dielectric disk made out of silicon (gray) placed on a quartz substrate (blue). E-field at center XY plane of the disk is projected above the disk (shown in red arrows). Induced dipole moment (shown in green arrow) is along the X direction. Inset: 2D cross-section of a unit cell with R = 315 nm, c = 165 nm, a1 = 230 nm, b1 = 90 nm, t1 = 115 nm, L1 = 750 nm. c) Experimental (dashed) and simulated (solid) S-parameter curves for E-field polarized along the Y direction. d) Experimental (dashed) and Simulated (solid) S-parameter curves for E-field polarized along the X direction. e) Zoom in of the calculated dimensionless electric surface susceptibility for the E-field polarized along the Y direction. No electric response is evoked since the induced electric dipole moment is orthogonal to the incident E-field. f) Zoom in of the calculated dimensionless electric surface susceptibility for the E-field polarized along the X direction. A strong electric response is evoked since the induced electric dipole is along the incident E-field.

Adv. Optical Mater. **2015**,
DOI: 10.1002/adom.201500222

The mode has a circulating electric field and does not radiate via an electric moment without the slot. The disk however, does radiate via a magnetic moment perpendicular to the plane of the disk (Z direction, Figure 1b). Nevertheless, the incident H-field is along the radial direction of the slab (Y direction, Figure 1b) and cannot couple to the magnetic moment arising from the Mie mode. Hence, for the purpose of discussion, this mode can be considered dark for the given incident direction. The quality factor (Q-factor) of the dark Mie mode is limited by the radiating magnetic moment and fabrication imperfections (since silicon is lossless around 1.55 μm). To generate an electric response function from the homogeneous disk, we place an off-centered slot with its axis along the Y direction (inset Figure 1b) creating an asymmetry in the structure. The slot serves to scatter light into the dark mode and in turn gets polarized due to the strong fields inside the disk, resulting in an induced electric dipole moment, perpendicular to the axis of the slot (X direction). The projected E-fields (red arrows, Figure 1b) at the center plane of the disk show high electric field magnitude inside the slot, indicating high residual polarization. For an incident electric field oriented perpendicular to the axis of the slot (X direction, Figure 1b) coupling is the most efficient and results in a strong electric response at 202 THz (Figure 1d,f). Upon changing the E-field polarization to the Y direction (Figure 1b), the resonance disappears, resulting in a negligible dipole moment (Figure 1c,e). Absorption for the case of E-field polarized along the Y direction is less than 10%. However, for the resonant case of E-field polarized along the X direction, absorption is around 24%. Experimental results agree well with the simulated results (Figure 1c,d), but the higher than expected absorption is most likely due to the fabrication imperfections and surface state absorption in the silicon. The physical thickness of the structure is 115 nm ≈ $\lambda_0/13$ (λ_0 is the free space wavelength at the resonance), which is deep subwavelength for propagation along the Z direction (compare with ≈ $\lambda_0/9$ thickness of a radiating electric resonance in a disk, Figure S1, Supporting Information). The disks can be made even thinner in the Z direction by stretching them along the lattice direction (X and Y). However, care must be taken to keep the lattice size sufficiently small so as to avoid higher diffraction orders. This scaling is true for all the meta-atoms presented in this work. The methodology presented here is similar to a metallic split ring resonator exhibiting circulating current in a ring with a capacitive gap.[1]

3. Polarization Dependent Magnetic Response

The second response in consideration is negative magnetic susceptibility. We use the same dark state in the silicon cylindrical disk as presented in the previous section. To generate a magnetic response, we require a loop with circulating current, similar to how magnetic resonances have been implemented in cut-wire pairs and fishnets.[7,8] To achieve this current loop, we place two scatterers diagonally across the cylindrical disk resulting in the excitation of the dark mode (exploded view inset **Figure 2**a). The nonresonant scatterers are shaped as thin semicylindrical disks, also made out of silicon. The projected uniform E-field at the center plane of the slab indicates net zero electric dipole moment (red arrows Figure 2a). This is a direct consequence of the symmetric placement of scatterers about the center axis of the disk (green plane in inset Figure 2a). In spite of the symmetry, the meta-atom still exhibits a magnetic dipole moment along the Y direction (green arrow Figure 2a). A scatterer, placed on top of the cylindrical disk (Figure 2a) gets polarized by the strong near-field of the dark resonator. Similarly, an induced polarization occurs in the scatterer, placed below the cylindrical disk. However, since the scatterers are placed on the opposite half of the dark cylindrical resonator, antiparallel displacement currents arise (see electric displacement field D plotted as golden arrows Figure 2a). The induced polarization currents in the semicylindrical scatterers are in different XY planes, separated by the thickness of the dark resonator, thereby generating a circulating current loop with its magnetic moment pointing along the incident H-field (Y direction in Figure 2a). Simulated results indicate magnetic sheet susceptibility at 209 THz accompanied by a narrow line-width resonance, for the incident H-field polarized along the Y direction (E_x, H_y in Figure 2c,e). Flipping the incident H-field along the X direction (E_y, H_x in Figure 2b,d) results in net-zero response from the meta-atom. The physical thickness of the meta-atom is 115 nm ≈$\lambda_0/12.4$, which is again deep subwavelength for a wave propagating along the Z direction (compare with ≈ $\lambda_0/7$ thickness of a radiating magnetic resonance in a disk, Figure S2, Supporting Information). We therefore have created a low loss dielectric equivalent of a cut-wire pair.

4. Polarization Independent Electric Response

In the previous sections, we have described a general method to excite a purely electric or magnetic response, sensitive only to a single incident polarization. However, to improve the practical applicability of our metamaterial, polarization independent structures are required (invariant response for E-field along either X or Y direction). The cylindrical geometry shown in Figures 1 and 2 cannot yield a polarization invariant response without converting a certain fraction of the incident light to cross-polarized transmittance (see Figures S3 and S4, Supporting Information). This is undesirable for many metamaterial applications. To mitigate this problem, we switch from a cylindrical to a rectangular geometry which allows us to decouple the response in orthogonal directions.

The second dark mode in consideration is the lowest order index guided TE mode in an infinite planar dielectric slab.[31] Guided modes in planar dielectric slab with holes have been studied quite extensively in the past.[32] We revisit such structures in the context of metasurfaces exhibiting electric response.

The fabricated structure consists of a planar silicon thin film ($\varepsilon \approx 13.69$, t2 = 115 nm) with a cross slot scatterer, etched through the center of a square lattice (**Figure 3**a,b, inset). The excited mode profile along the X/Y direction is TE (2, 0) and is fixed by the lattice constant (L3 in Figure 3b). This mode cannot be excited from free space without scatterers, due to the field symmetry of the mode about the XZ plane. Therefore, this mode has no radiation via either electric or magnetic dipole moments and it is perfectly dark (as opposed to the homogeneous disks which possess a radiating magnetic moment

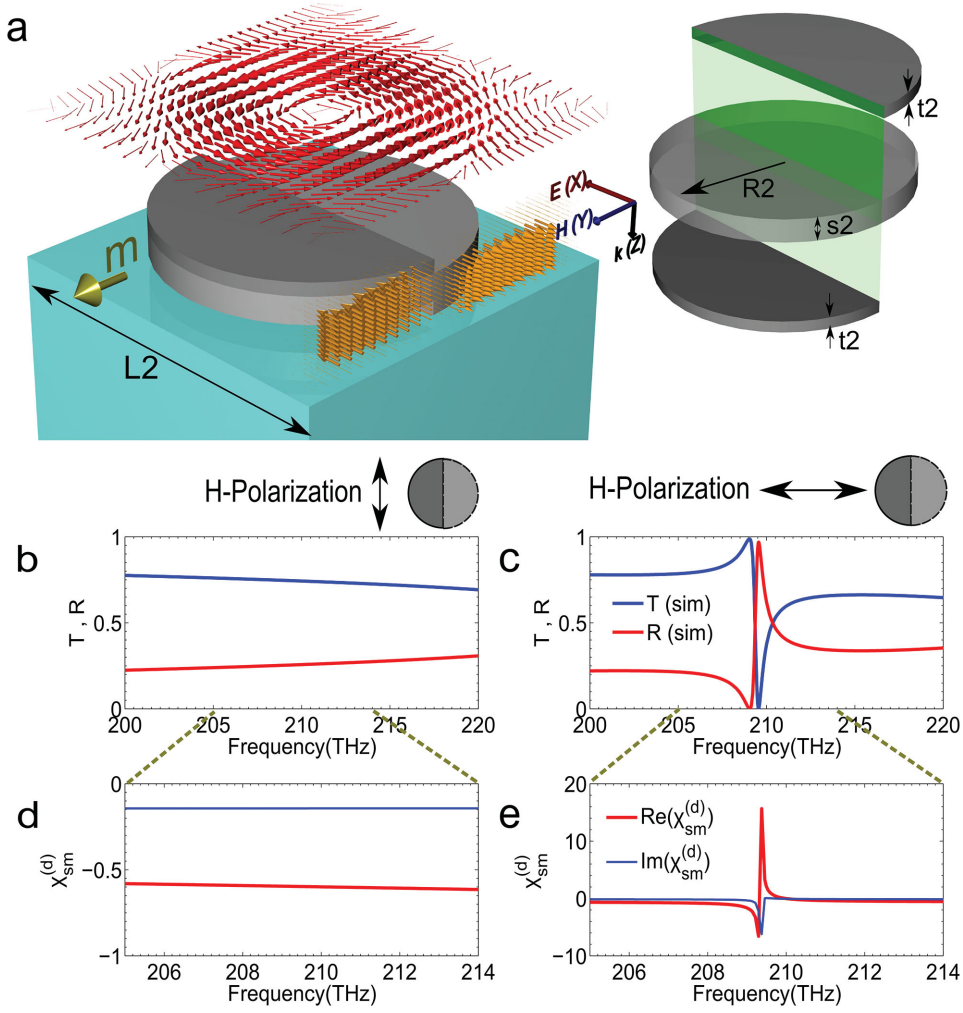

Figure 2. Polarization sensitive magnetic response of a dielectric disk with a semicylindrical disk scatterer. a) Simulated unit cell of the proposed design with the dielectric disk made out of silicon (gray) placed on quartz substrate (blue). Semicylindrical scatterers are placed diagonally across the slab. E-field at the center XY plane of the disk is projected above the disk (shown in red arrows). Uniform fields indicate zero electric dipole moment. Golden arrows indicate the projected D-field inside the material at the center YZ plane of the disk. Antiparallel fields in the scatterers generate a magnetic dipole moment (shown in green arrow). Inset: Exploded view of the magnetic meta-atom, *R*2 = 315 nm, t2 = 30 nm, s2 = 55 nm, L2 = 750 nm. The semitransparent green plane indicates the center plane of the disk. b) Simulated S-parameter curves for E-field polarized along the Y direction. c) Simulated S-parameter curves for H-field polarized along the X direction. d) Zoom in of the calculated effective magnetic susceptibility for the H-field polarized along the X direction. No magnetic response is evoked since the induced magnetic dipole moment is orthogonal to the incident H-field. e) Zoom in of the calculated effective magnetic susceptibility and the figure of merit for the H-field polarized along the Y direction. A strong magnetic response is evoked since the induced magnetic dipole moment (m) is along the incident H-field.

perpendicular to the plane of the slab). It is also important to note that the infinite extent of the thin film (along X and Y direction Figure 3b) allows us to have degenerate versions of the TE (2, 0) mode, whose excitation is dependent on the placement of the scatterers. We appropriately place our scatterers so as to excite only one degenerate mode for a given response. For a given lossless material, the Q-factor of these modes is purely limited by the fabrication imperfections only. To create a polarization independent electric response, we etch a symmetric rectangular slot through the center of the unit cell. To maintain a polarization independent response, we rotate the slot by 90° about the center of the unit cell. Superposition of these two orthogonal slots results in a cross structure (Figure 3a,b, inset). The projected E-field at the center of the slab (red arrows in Figure 3b) shows the TE (2, 0) mode excited in the resonator. The mode is symmetric ($TE^{symmetric}$ (2, 0)) with respect to the slot axis (inset of Figure 3b). The slot with its axis along the Y direction couples to an incident E-field along the X direction only and vice versa (see projected E-field Figure 3b; stronger fields above the slot indicate a residual electric polarization). The simulated and corresponding experimental results for the cross structure clearly show the approximately similar transmittance and reflectance for both X and Y polarized E-fields (Figure 3c,d). The calculated dimensionless electric sheet susceptibility from the simulations also remains invariant under the polarization change (Figure 3e,f), thus confirming our approach. The larger damping of the experimentally measured resonances with respect to the simulations can be attributed

Adv. Optical Mater. **2015**,
DOI: 10.1002/adom.201500222

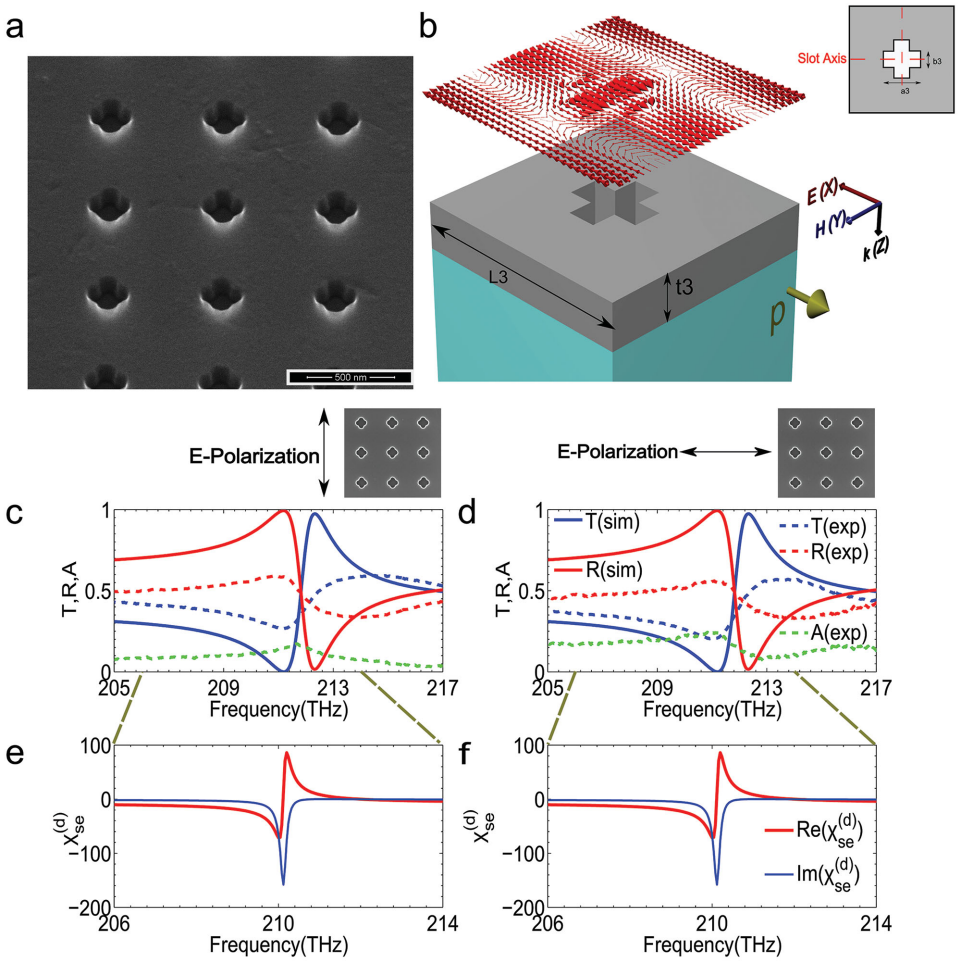

Figure 3. Polarization independent electric response of a dielectric slab with a cross scatterer. a) SEM image of a single layer dielectric slab with periodically repeated cross scatterers. b) Simulated unit cell of the proposed design consisting of a dielectric slab made out of silicon (gray) placed on a quartz substrate (blue). The cross slot scatterer is fabricated at the center of the unit cell by superimposing two orthogonal rectangular slots. Projected E-field at the center XY plane of the slab (shown in red arrows) showing a strong field inside the cross, inducing an effective electric dipole moment (p shown in green arrow) along the X direction. If the incident E-field is switched to the Y direction (not shown in this figure), similar response is obtained due to the symmetry of the structure. Inset: 2D cross-section of the unit cell with a3 = 230 nm, b3 = 90 nm, t3 = 115 nm, L3 = 620 nm. c) Experimental (dashed) and simulated (solid) S-parameter curves for E-field polarized along the Y direction. d) Experimental (dashed) and simulated (solid) S-parameter curves for E-field polarized along the X direction. e) Zoom in of the calculated dimensionless electric surface susceptibility for the E-field polarized along the Y direction. A strong electric response is evoked since the induced electric dipole moment is along the incident E-field. f) Zoom in of the calculated dimensionless electric surface susceptibility for E-field polarized along the X direction. A strong electric response is evoked in the same manner as the response obtained for E-field polarized along the Y direction.

to increased loss in the silicon arising due to the etch process as well as roughness in the patterned areas. These losses are also indicated by the increased absorption in Figure 3c,d. This approach is quite similar to how surface plasmon polaritons in thin metallic films are coupled to free space via a grating.[33]

5. Polarization Independent Magnetic Response

To excite a polarization independent magnetic response with a planar dielectric slab, we essentially follow the same approach used with a disk resonator. A thin silicon slab, half the width of the unit cell is used as a scatterer. These scatterers are placed diagonally across the thick dielectric slab (inset of **Figure 4**a). As before, we rotate the scatterers by 90° about the center plane of the unit cell. The original pair of scatterers along with the rotated counterpart is superimposed together to arrive at an L shaped scatterer (Figure 4a). An important thing to note here is that the excited dark mode differs from the polarization independent electric response case (compare red E-field arrows in Figure 3b with red E-field arrows in Figure 4a). The mode profile in the Y direction is antisymmetric ($TE^{antisymmetric}$ (2,0)) with respect to the slot axis (semitransparent green plane in Figure 4a, inset). Only the $TE^{antisymmetric}$ (2, 0) mode contributes to the response for the current arrangement of scatterers. Simulated D-fields (golden arrows in Figure 4a) indicate that the current flow in the top and bottom scatterer is antiparallel. As these currents lie along different XY planes, a magnetic moment m_y (green arrow, Figure 4a) is generated for an incident E_x field and vice versa. The simulation results

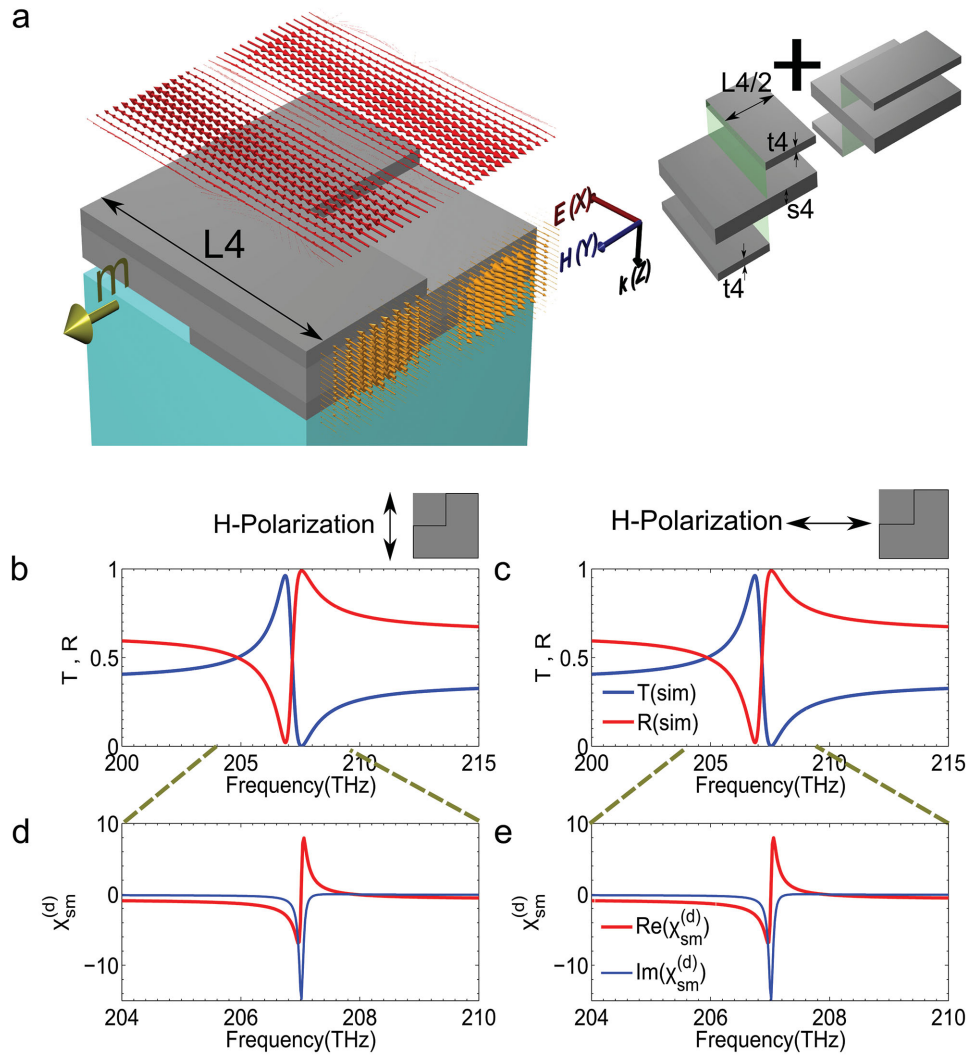

Figure 4. Polarization independent magnetic response of a thick dielectric slab with a thin slab scatterer. a) Simulated unit cell of the proposed design with a dielectric slab made out of silicon (gray) placed on a quartz substrate (blue). The scatterers are made out of the thin slab, half the width of unit cell, and are placed diagonally across the slab. The E-field at the center XY plane of the thicker slab is projected above (shown in red arrows). Uniform fields indicate zero electric dipole moment. Golden arrows indicate the projected D-field inside the material at the center YZ plane of the disk. Antiparallel fields in the out of plane scatterers generate a magnetic dipole moment (m shown in green arrow). Inset: Exploded view of the magnetic meta-atom L4 = 620 nm, t4 = 30 nm, s4 = 55 nm. The semi-transparent green plane indicates the center plane of the thick slab b) Simulated S-parameter curves for H-field polarized along the Y direction. c) Simulated S-parameter curves for H-field polarized along the X direction. d) Zoom in of the dimensionless magnetic sheet susceptibility for the H-field polarized along the Y direction. e) Zoom in of the dimensionless magnetic sheet susceptibility for the H-field polarized along the X direction.

and the retrieved dimensionless magnetic sheet susceptibility (Figure 4b,c,d,e) clearly indicate an equivalent magnetic response for E-field polarized either along the X or Y direction.

In order to fabricate the structures possessing magnetic resonances, depicted in Figures 2 and 4, a multistep lift-off and deposition procedure can be utilized. In this case, the first layer is patterned via electron beam lithography followed by deposition of the resonator material and planarization. Planarization would involve deposition or spinning of a transparent low index medium, such as SiO_2 or a polymer. This layer would then be planarized level with the resonator via mechanical or chemical polishing. The subsequent layers would then be aligned, overlaid, and planarized to form the multilayer resonators.

6. Conclusion

We have theoretically and experimentally demonstrated a method to design subwavelength dielectric metamaterials by splitting the response into two components. The first component consists of a nonradiative or dark resonator, which stores the major fraction of the electromagnetic energy. The second component is the nonresonant scatterer, which imparts this dark-resonator its desired response. The response can be easily altered by changing the geometry of the scatterers. Thus, other responses such as chirality or nonlinearity can be obtained by a judicious choice of the scatterers.[34,35] This approach is significantly different from regular metamaterial structures where

Adv. Optical Mater. 2015,
DOI: 10.1002/adom.201500222

a single resonator stores and dissipates energy due to finite polarizability of the structure. In this work, we decouple the response of the resonator from its geometry, which imparts greater versatility to the design process. The magnitude of the response can be tuned by simply changing the coupling between the dark mode resonator and the scatterer (changing thickness or radius/width of scatterer). The principles presented in this article can be extended to any structure with negligible dipole moment. Approaches such as conformal mapping might enable more complex geometries with deeper subwavelength meta-atoms.[36,37] The electromagnetic response of existing dark metallic meta-atoms[38,39] can also be altered using this approach, provided loss can be compensated by gain.[39–42] This method is not limited to classical resonators and atomic transitions can also be used,[43] if an appropriate scatterer is available. The reduction of dissipation and compact dimensions in dielectric metasurfaces is very desirable for applications involving a normally incident beam, such as slow light devices, modulators, nonlinear frequency conversion, polarization convertors or optical isolation. Thus, our work offers a method to enable these applications at much higher frequencies and with much more compact geometries.

7. Experimental Section

Sample Fabrication: Amorphous Si (α-Si) of thickness 115 nm was deposited on an RCA-cleaned quartz substrate using low pressure chemical vapor deposition (LPCVD). The substrate was then spin coated with A2 PMMA (950K, Microchem Corp.) at 2000 rpm and electron beam lithography (Raith) was carried out to write a pattern area of 100 × 100 μm. After pattern development, PMMA was used as the mask for subsequent reactive ion etching (RIE) of the α-Si using a SF6/C4F8 recipe in an Oxford Plasma Lab etcher. The PMMA mask was then removed using oxygen plasma etch followed by heating (60 °C) the sample in acetone. α-Si, deposited at the backside of the substrate, was removed by the same SF6/C4F8 recipe that was used for etching the resonators.

Optical Characterization and Effective Parameter Retrieval: Broadband reflectance (R) and transmittance (T) were measured by focusing white light (Tungsten/Halogen lamp) on the patterned array through an infrared objective with a low numerical aperture (Mitutoyo, 20×, NA 0.40). The incident angle was further restricted by placing an aperture in the back focal plane of the objective. Transmitted light was collected using a 50× infrared objective with the same numerical aperture (NA 0.40) as the objective for incident light. The reflectance and transmittance spectra were measured using a spectrometer (Horiba, Jobin Yvon) with an InGaAs detector. The baseline reflectance and transmittance were measured using a silver mirror and a quartz wafer, respectively. In order to ensure that there was no high angle scattered light coming from the sample, a high numerical aperture infrared objective (Nikon, 60×, NA 0.95) was also used to collect the transmitted light. However, no difference in transmission was measured between the low and high NA collection optics, indicating weak scattering. The absorbance (A) is calculated from the measured reflectance and transmittance as $A = 1\text{-}R\text{-}T$. The refractive index of the LPCVD deposited α-Si film was measured using a spectroscopic ellipsometer (Wollam Co. Inc.). All susceptability calculations are based on references.[44,45]

Supporting Information

Supporting Information is available from the Wiley Online Library or from the author.

Acknowledgements

Work at Ames Laboratory was in part supported by the U.S. Department of Energy, Office of Basic Energy Science, Division of Materials Sciences and Engineering, Contract No. DE-DE-AC02-07CH11358 (theory), and by the US office of Naval Research, Award No. N00014-14-1-0474 (simulation) and Award No. N00014-14-1-0475 (experiments). This work was partially supported by European Research Council under the ERC Advanced Grant No. 320081(PHOTOMETA).

Received: April 27, 2015
Revised: May 30, 2015
Published online:

[1] D. R. Smith, J. B. Pendry, M. C. K. Wiltshire, *Science* **2004**, *305*, 788.
[2] W. Cai, V. M. Shalaev, *Optical Metamaterials: Fundamentals and Applications*, Springer-Verlag, New York **2010**.
[3] C. M. Soukoulis, S. Linden, M. Wegener, *Science* **2007**, *315*, 47.
[4] Y. Liu, X. Zhang, *Chem. Soc. Rev.* **2011**, *40*, 2494.
[5] C. M., Soukoulis, M. Wegener, *Nat. Photonics* **2011**, *5*, 523.
[6] S. Linden, C. Enkrich, M. Wegener, J. Zhou, T. Koschny, C. M. Soukoulis, *Science* **2004**, *306*, 1351.
[7] G. Dolling, M. Wegener, C. M. Soukoulis, S. Linden, *Opt. Lett.* **2007**, *32*, 53.
[8] J. Valentine, S. Zhang, T. Zentgraf, E. Ulin-Avila, D. A. Genov, G. Bartal, X. Zhang, *Nature* **2008**, *455*, 376.
[9] N. I. Landy, S. Sajuyigbe, J. J. Mock, D. R. Smith, W. J. Padilla, *Phys. Rev. Lett.* **2008**, *100*, 207402.
[10] H. Suchowski, K. O'Brien, Z. J. Wong, A. Salandrino, X. Yin, X. Zhang, *Science* **2013**, *342*, 1223.
[11] S. Liu, M. B. Sinclair, T. S. Mahony, Y. C. Jun, S. Campione, J. Ginn, D. A. Bender, J. R. Wendt, J. F. Ihlefeld, P. G. Clem, J. B. Wright, *Optica* **2014**, *1*, 250.
[12] M. Esfandyarpour, E. C. Garnett, Y. Cui, M. D. McGehee, M. L. Brongersma, *Nat. Nanotechnol.* **2014**, *9*, 542.
[13] X. Yang, J. Yao, J. Rho, X. Yin, X. Zhang, *Nat. Photonics* **2012**, *6*, 450.
[14] P. Moitra, Y. Yang, Z. Anderson, I. I. Kravchenko, D. P. Briggs, J. Valentine, *Nat. Photonics* **2013**, *7*, 791.
[15] N. Liu, L. Langguth, T. Weiss, J. Kästel, M. Fleischhauer, T. Pfau, H. Giessen, *Nat. Mater.* **2009**, *8*, 758.
[16] N. Yu, F. Capasso, *Nat. Mater.* **2014**, *13*, 139.
[17] N. Yu, P. Genevet, M. A. Kats, F. Aieta, J. P. Tetienne, F. Capasso, Z. Gaburro, *Science* **2011**, *334*, 333.
[18] J. Zhou, T. Koschny, M. Kafesaki, E. N. Economou, J. B. Pendry, C. M. Soukoulis, *Phys. Rev. Lett.* **2005**, *95*, 223902.
[19] S. O'Brien, J. B. Pendry, *J. Phys. Condens. Matter* **2002**, *14*, 4035.
[20] Q. Zhao, J. Zhou, F. Zhang, D. Lippens, *Mater. Today* **2009**, *12*, 60.
[21] I. B. Vendik, O. G. Vendik, M. S. Gashinova, *Tech. Phys. Lett.* **2006**, *32*, 429.
[22] L. Peng, L. Ran, H. Chen, H. Zhang, J. Kong, T. Grzegorczyk, *Phys. Rev. Lett.* **2007**, *98*, 157403.
[23] Q. Zhao, L. Kang, B. Du, H. Zhao, Q. Xie, X. Huang, B. Li, J. Zhou, L. Li, *Phys. Rev. Lett.* **2008**, *101*, 027402.
[24] J. C. Ginn, I. Brener, D. W. Peters, J. R. Wendt, J. O. Stevens, P. F. Hines, L. I. Basilio, L. K. Warne, J. F. Ihlefeld, P. G. Clem, M. B. Sinclair, *Phys. Rev. Lett.* **2012**, *108*, 097402.
[25] A. I. Kuznetsov, A. E. Miroshnichenko, Y. H. Fu, J. B. Zhang, B. Luk'yanchuk, *Sci. Rep.* **2012**, *2*, 492.
[26] A. B. Evlyukhin, S. M. Novikov, U. Zywietz, R. L. Eriksen, C. Reinhardt, S. I. Bozhevolnyi, B. N. Chichkov, *Nano Lett.* **2012**, *12*, 3749.

[27] I. Staude, A. E. Miroshnichenko, M. Decker, N. T. Fofang, S. Liu, E. Gonzales, J. Dominguez, T. S. Luk, D. N. Neshev, I. Brener, Y. Kivshar, *ACS Nano* **2013**, *7*, 7824.
[28] M. Decker, I. Staude, M. Falkner, J. Dominguez, D. N. Neshev, I. Brener, T. Pertsch, Y. S. Kivshar, *Adv. Opt. Mater.* **2015**, *3*, 813.
[29] Y. Yang, I. I. Kravchenko, D. P. Briggs, J. Valentine, *Nat. Commun.* **2014**, *5*, 5753.
[30] S. Zhang, D. Genov, Y. Wang, M. Liu, X. Zhang, *Phys. Rev. Lett.* **2008**, *101*, 47401.
[31] K. Sakoda, *Optical Properties of Photonic Crystals*, Springer-Verlag, Berlin **2001**, Ch. 8.
[32] S. Fan, J. D. Joannopoulos, *Phys. Rev. B* **2002**, *65*, 235112.
[33] S. A. Maier, *Plasmonics: Fundamentals and Applications*, Springer-Verlag, Berlin **2007**, Ch. 3.
[34] E. Plum, J. Zhou, J. Dong, V. A. Fedotov, T. Koschny, C. M. Soukoulis, N. I. Zheludev, *Phys. Rev. B* **2009**, *79*, 035407.
[35] Y. S. Kivshar, *Adv. Natl. Sci.: Nanosci. Nanotechnol.* **2014**, *5*, 013001.
[36] J. Zhang, A. Zayats, *Opt. Express* **2013**, *21*, 8426.
[37] A. C. Atre, A. G. Etxarri, H. Alaeian, J. A. Dionne, *Adv. Opt. Mater.* **2013**, *1*, 327.
[38] D. O. Güney, T. Koschny, C. M. Soukoulis, *Phys. Rev. B* **2011**, *83*, 045107.
[39] A. Boltasseva, H. A. Atwater, *Science* **2011**, *331*, 290.
[40] O. Hess, J. B. Pendry, S. A. Maier, R. F. Oulton, J. M. Hamm, K. L. Tsakmakidis, *Nat. Mater.* **2012**, *11*, 573.
[41] A. N. Lagarkov, V. N. Kisel, A. K. Sarychev, *J. Opt. Soc. Am. B* **2010**, *27*, 648.
[42] Z. Huang, T. Koschny, C. M. Soukoulis, *Phys. Rev. Lett.* **2012**, *108*, 187402.
[43] S. E. Harris, *Phys. Today* **1997**, *50*, 36.
[44] C. Holloway, E. Kuester, A. Dienstfrey, *IEEE Antennas Wireless Propag. Lett.* **2011**, *10*, 1507.
[45] M. Albooyeh, D. Morits, C. R. Simovski, *Metamaterials* **2011**, *5*, 178.

Adv. Optical Mater. **2015**,
DOI: 10.1002/adom.201500222